MEASUREMENT OF THE BREMSSTRAHLUNG SPECTRUM OF THE LINEAR ACCELERATOR

William J. Sawtelle

Library
U. S. Naval Postgraduate School
Monterey, California

The author wishes to express his sincere appreciation to Dr. C. P. Sargent for his guidance and interest in all phases of this experiment; and to others in the linear accelerator group for their assistance and very pleasant association.

The editor wishes to express his sincere
appreciation to Mr. C. F. Sargent for his gracious
aid and interest in all phases of this enjoyable
work and to others in the Illumat Laboratory
Group for their assistance and very pleasant
association.

MEASUREMENT OF THE BREMSSTRAHLUNG SPECTRUM OF THE LINEAR ACCELERATOR

by

WILLIAM J. SAWTELLE

SUBMITTED TO THE DEPARTMENT OF PHYSICS
ON 23 MAY 1955 IN PARTIAL FULFILLMENT
OF THE REQUIREMENTS FOR THE DEGREE OF
MASTER OF SCIENCE

An X-ray spectrometer designed to monitor the bremsstrahlung beam of the MIT linear accelerator has been designed and tested. This spectrometer measures the energy distribution of the photo protons from deuterium. The bremsstrahlung spectrum is found by using the known cross section for the d(,n)p reaction. The efficiency of the monitor is about 10^{-9} protons per photon which is sufficient to monitor some of the experiments planned for the linear accelerator.

Thesis Supervisor.....Bernard T. Feld
Associate Professor of Physics

Physics Department.....Bernard I. Polk
Research Physicist at Polytex

MEASUREMENT OF THE BREMSSTRAHLUNG SPECTRUM OF THE LINEAR ACCELERATOR

by

WILLIAM J. SAWTELLE

B. S., UNITED STATES NAVAL ACADEMY 1949

SUBMITTED IN PARTIAL FULFILLMENT OF THE REQUIREMENTS FOR THE DEGREE OF

MASTER OF SCIENCE

at the

MASSACHUSETTS INSTITUTE OF TECHNOLOGY

June 1955

TABLE OF CONTENTS

PAGE

I INTRODUCTION.....1

II THE MONITOR.....3

III ELECTRONICS.....7

IV GENERAL DISCRIPTION OF EXPERIMENT.....9

V RESULTS.....11

VI CONCLUSIONS.....24

FIGURES

1. General Construction of Monitor Box.....6a
2. Block Diagram of Electronic Equipment.....8a
3. General Layout of Experiment.....10a
4. Typical Calibration Curve.....12a
5. Counts vs Pulser Volts
   a. Run I.....14a
   b. Run II.....14b
   c. Run III.....14c
6. Proton Counts versus Pulser Volts.....15a
7. Protons per Mev versus Proton Energy for Run II.....21a
8. Cross section curve for d(γ,n)p.....22a
9. Photons per Mev versus Photon Energy
   a. Run I and Run III.....23a
   b. Run II.....23b

APPENDICES

I. Resolution.....25

II. The cross section of the $Cu^{63}(\gamma,n)Cu^{62}$ reaction at 19 Mev.....29

REFERENCES.....34

28783

TABLE OF CONTENTS

PAGE

I 1

II 5

III 7

IV 11

V 12

VI 14

FIGURES

1. 16
2. 16
3. 16
4. 16
5. 16
6. 16
7. 16
8. 16
9. 16
10. 16
11. 16
12. 16

APPENDICES

I. 30
II. 30

..... 30

..... 34

I Introduction

The M.I.T. linear accelerator produces pulses of electrons at a repetition rate of 120 pulses per second in one micro-second bursts. The electron energies range from six to about seventeen Mev at currents of about 2 micro amperes. The electron energy spectrum is about 25% wide at its half maximum. For experiments done with the linear accelerator the electrons produce bremsstrahlung in a heavy target and the X-ray beam is used for the experiment. Because the electrons have a rather wide spectrum and the energy and current vary from time to time during a run, it is desirable to monitor the X-ray beam with an energy sensitive detector. It is the purpose of this thesis to design and calibrate a monitor which will measure the bremsstrahlung spectrum.

The cross section for the photodisentegration of deuterium has been measured to within 10% in the photon energy range from 2.227 to 20 Mev.[1,2,3] By determining the proton energy spectrum from the photodisentegration of deuterium and by using the known cross section for this reaction, ie. $d(\gamma,n)p$, the bremsstrahlung spectrum can be determined. The monitor will consist of a box filled with deuterium, a scintillator to detect protons, and suitable electronics to analyse the proton distribution.

I Introduction

II The Monitor

For structural details of the monitor box see figure 1.

Since the maximum energy of the linear accelerator is about 17 Mev the maximum photon energy will be about 17 Mev. Seventeen Mev photons will produce protons from the photodisentegration of deuterium having an energy of about 7-8 Mev: $h\nu \approx 2T_p + 2.227$ Mev, where Tp is the kinetic energy of the proton and 2.227 Mev, is the binding energy of the deuteron.

To detect protons a scintillator will be used. Such a scintillator will have to be thick enough to stop 8 Mev protons. A scintillator will also be sensitive to electrons, and therefore indirectly to photons, and must, therefore, be shielded. No shielding can be used in front of the scintillator since it is desired to detect protons. In order that pulse heights from electrons be kept as low as possible, the scintillator must be made as thin as possible, the minimum thickness being that which will just stop 8 Mev protons.

The first question to be answered was what type of scintillator to use. For ease of handling as well as having a fast decay time so that the effect on resolution of pile up of small pulses can be minimized, anthracene appeared to be best. However its proton pulse height to electron

pulse height ratio for same energy loss is only about .3 at 2 Mev and the crystal is non linear to protons. A proton of 1 Mev does not give half the pulse height of a 2 Mev proton.

NaI(Tl) has a slower decay time than anthracene and is harder to handle because of its deliquisent property but it is linear to protons and yields equal size pulses for equal energy loss by protons and electrons. The counting rates are sufficiently low that pile up is no problem, and NaI(Tl) does not need to be shielded from fast neutrons. NaI(Tl) was chosen for the scintillator.

A thickness of .025 inches was used and corresponds to a loss of about .4 Mev for minimum ionizing electrons entering the crystal perpendicularly. The crystal was filed down to about .075 inches from a thicker slice and was then thinned down to final thickness by using butyl alcohol. The crystal was then placed in oil (Nujol) until ready to be used.

A 18 inch long aluminum tube was placed on the entrance window of the box to move the aluminum entrance window as far as possible from the crystal. Electrons from this window are swept out of the beam by a magnet placed near the front of the tube.

A 1" diameter lucite rod is used to transmit the light pulse from the crystal to the photo-multiplier tube (RCA5819). This rod runs through a hole in the side of the box and then through 1¼" diameter hole in a lead shielding block. A slot was cut in the lead block as shown in figure 1. An aluminum slide having four positions or "windows" is inserted into this slot. The slide contains three "windows" of varying thickness of aluminum, and one empty position. One position has 102 mg/cm^2 of aluminum which will stop 8 Mev protons, the other two positions have 6 mg/cm^2 and 25 mg/cm^2 aluminum. The "thick" window is used to measure background by preventing protons from reaching the counter, while effecting electrons and protons only slightly. The open window is used to make the proton runs.

Two NaI(Tl) crystals 1.21 and 1.10 square centimeters and each .06 centimeters thick were dipped in oil and laid on the end of the lucite light pipe and held there by the surface tension of the oil. Very thin (.26 mg/cm^2) aluminum leaf was then placed over the face of the crystal and the end of the light pipe and the excess oil pressed out. This aluminum leaf not only improved the light collecting efficiency but also helped protect the NaI(Tl) crystal. A small open can containing phosphorous pentoxide

was placed in the box to remove moisture, and the box was evacuated. The box was filled with one atmosphere of deuterium through a cold trap cooled by liquid nitrogen to remove any water vapor that might be present in the gas.

An alpha particle source in the form of thorium nitrate on a lucite plate is mounted in the box on an arm so that it can be moved in front of the crystal. This alpha particle source is used to check stability of light collecting efficiency and photomultiplier gain. The alpha particle spectrum was taken soon after the crystal was mounted and checked at intervals throughout the experiment. No deteriation of the crystal was observed over a period of 4 weeks, either by the alpha ray spectrum or visually.

The alpha source was prepared by dissolving thorium nitrate in alcohol and depositing this solution on a lucite plate. The alcohol was evaporated leaving a deposit of thorium nitrate of about 3 mg/cm^2.

X-ray film was used for final alignment of the box and to determine the size and position of the photon beam.

The front, sides, bottom, and top of the box were then covered with 7 inches of lead to reduce general background.

Figure 1: General Construction of Monitor Box

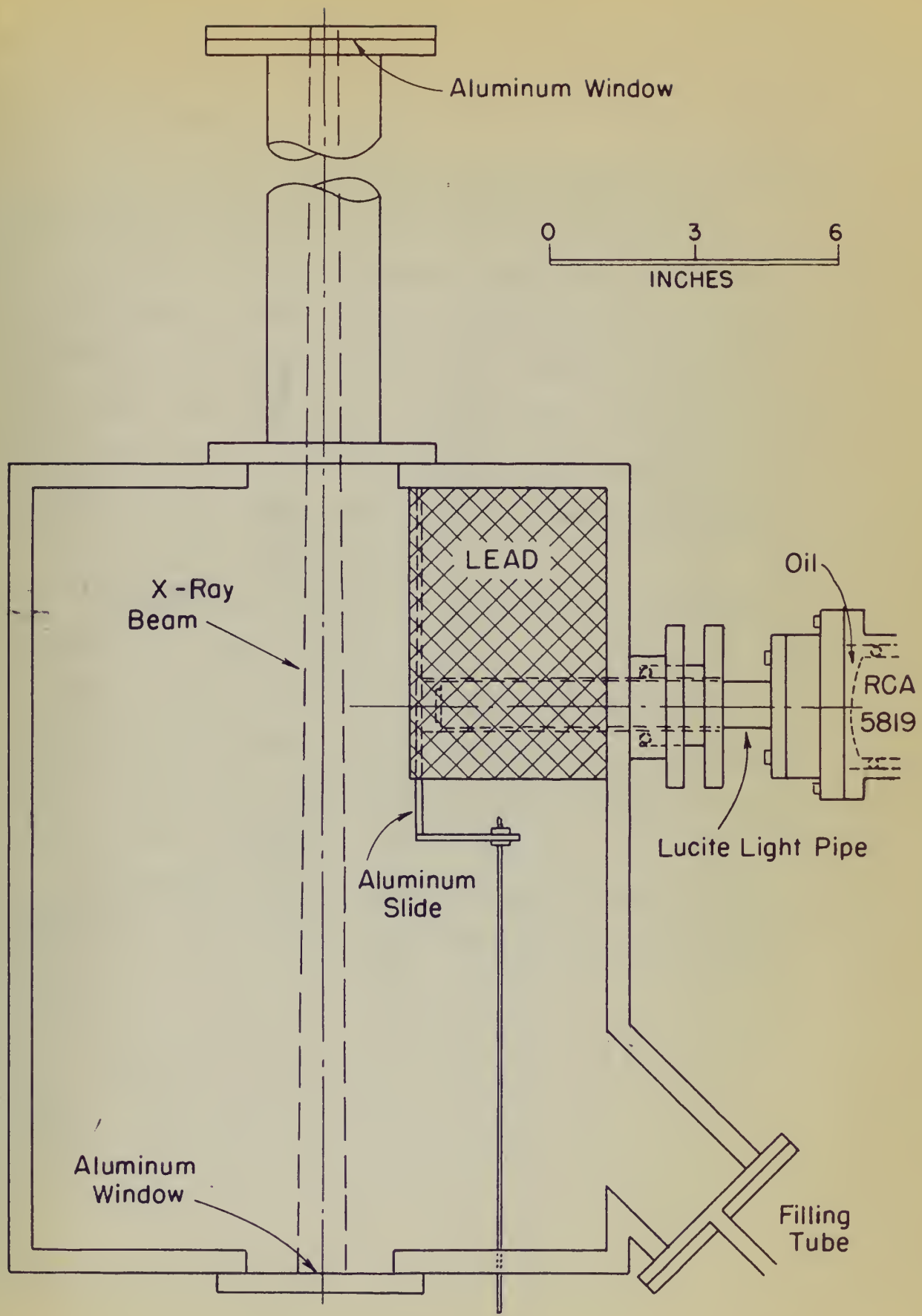

DETAILS OF BOX

Figure 1

III Electronics

The current pulse from the photomultiplier tube is amplified as near the phototube as possible to reduce the effect of radio frequency pickup from the linear accelerator. After initial amplification the pulse is transmitted to another amplifier near the analyzing circuit, (see figure 2). Pulses above some level, which is controlled by a discriminator, open a gate which allows the properly shaped pulse to enter the multi-channel pulse height analyzer.

The over-all electronic gain from the phototube through the pulse height analyzer is calibrated by mixing a signal from a W. E. 275 B pulser with the phototube signal at the input to the preamplifier. The over-all gain from pulser through pulse height analyzer is stable to 1% over a period of several hours.

The pulse height analyzer used is discribed in detail by J. E. Snyder, S.M. Thesis, MIT, June 1955.

Figure 2: Block Diagram of Electronic Equipment

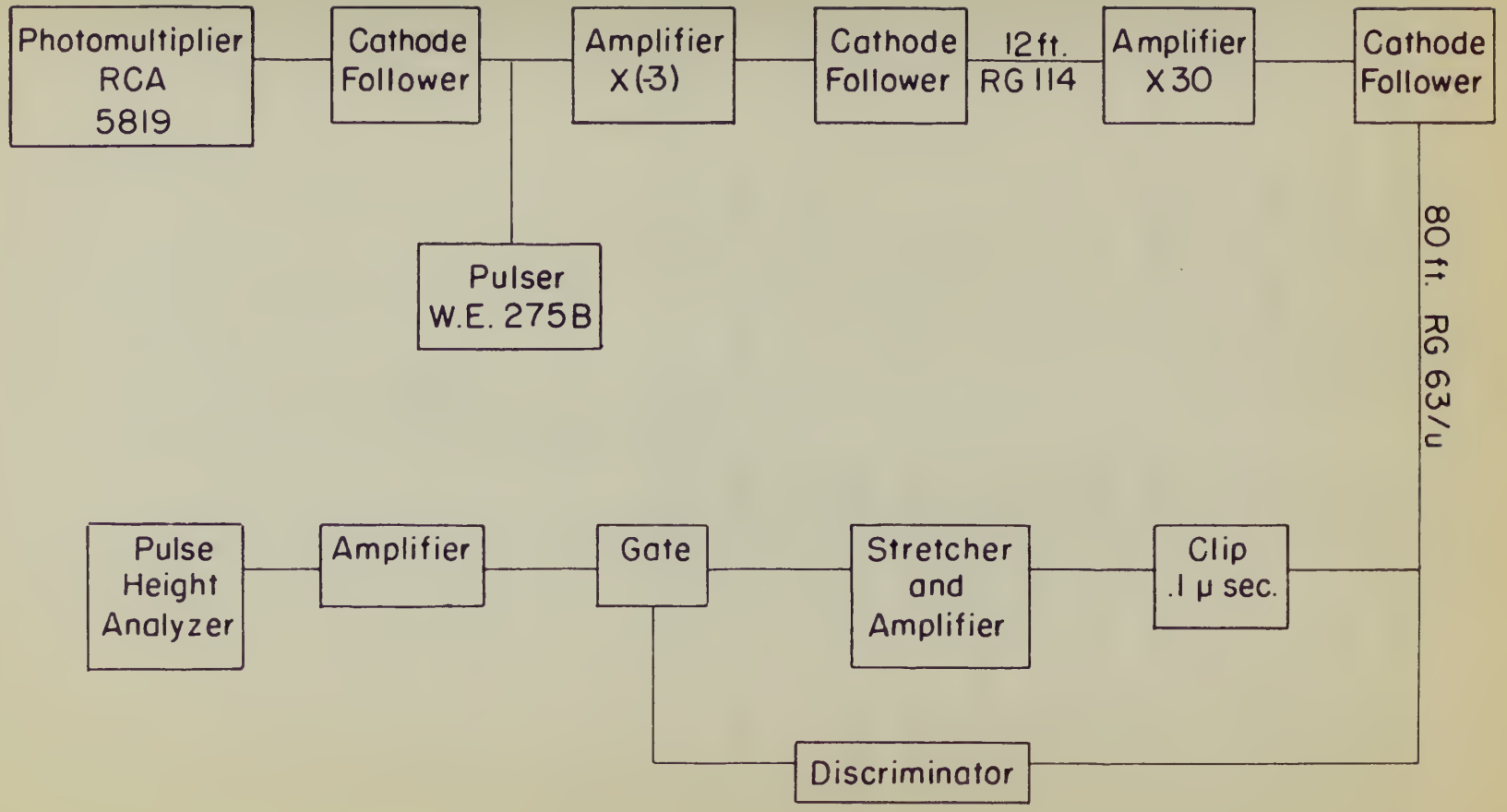

Figure 2

BLOCK DIAGRAM OF ELECTRONIC EQUIPMENT

IV General Discription of Experiment

The electrons from the linear accelerator were focused on a lead target by means of focusing coils. (See Figure 3). The target was located at the front of a 24" long $\frac{1}{4}$" diameter lead collimator. The photon beam emerging from the collimator entered the thin aluminum window on the front of the tube leading to the box. Electrons formed from the window were swept out of the beam by the sweeping magnet. The photon beam passed through the box and then, after some attenuation by several sheets of lead, its intensity was measured by a Beckman MX 3A ionization chamber. This meter was used to monitor the runs. The Beckman reading was kept about the same for the true runs and the background runs.

IV General Description of Equipment

The apparatus from the linear accelerator beam
focussed on a lead target by means of focusing units. (See
Figure 3). The target was located at the focus of a 90°
long 3" diameter lead collimator. The monitor beam emerg-
ing from the collimator intercepted the thin aluminum window
on the front of the ionization chamber box. Electrons
formed from the ionization gave rise to a flow of ions by
the sweeping voltage. The photon beam continued through the
box and then, after some attenuation by several inches
of lead, was incidently monitored by a Victoreen 6D 3%
ionization monitor. This helps was used to monitor the
beam. The monitor reading was kept about the same for
the runs with and the background runs.

Figure 3: General Layout of Experiment

Figure 3

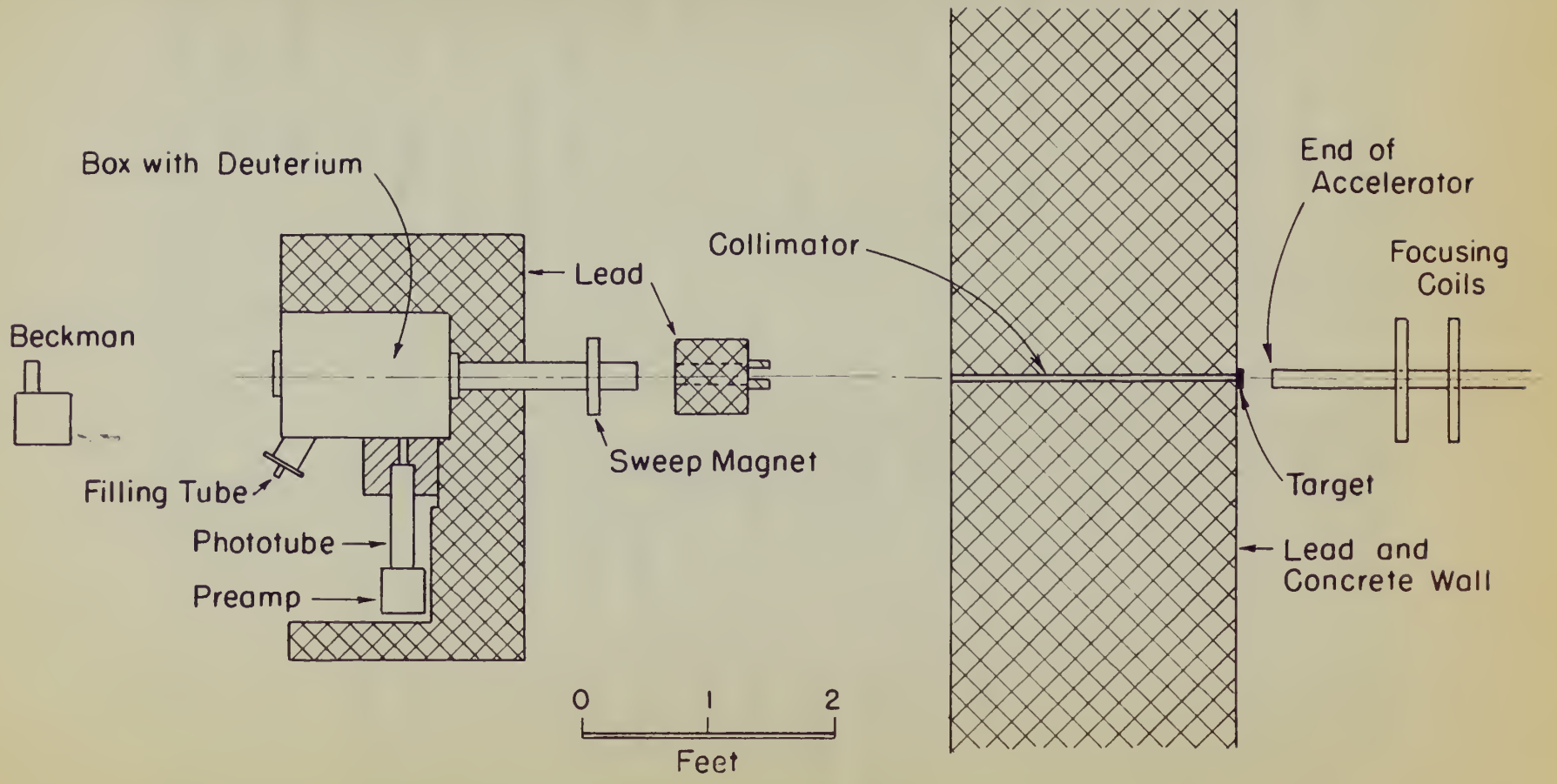

DIAGRAM OF EXPERIMENT

V Results

Three runs were made at three different maximum electron energies: Run I, 12 Mev; Run II, 14 Mev, and Run III, 16 Mev. For each run a one hour proton run was made, followed by a forty-five minute background run, and then another one hour proton run. The electron spectrum was checked before and after each part of the run. The spectrum was probably relatively constant during runs I and II, but drifted considerably during run III.

A proton run was a run in which the photo-protons were allowed to reach the scintillator; for the background runs the 102 mg per cm^2 aluminum absorber was between the X-ray beam and the crystal. This count difference gives, to a first approximation, the energy spectrum of the photo-protons from deuterium. The presence of the aluminum proton absorber should have some affect on electrons and photon background counts. To check this effect, runs were made with hydrogen rather than deuterium in the box, and it was found that the absorber actually reduced background by $20 \pm 10\%$. This correction was made on the background runs.

Before and after each run, analyzer bin number was calibrated as a function of pulser voltage (see figure 4).

A Results

Three runs were made at three different voltages
(positive electrode: Run 1, 12 mesh Pyx 17, 24 div, and
Run 111, 24 mesh. Five mesh grid a one inch carbon rod
was used, fastened by a tungsten-clad molybdenum rod,
and then another one inch carbon rod. The filaments
were chromium plated and silver-back clad at the ends. The
spectrum was periodically reinforced during runs 1
and 11, but shifted considerably during run 111.

A Perkins and Elmer 12 with its Littrow-prism
mode adjusted in reach, the sensitivity for the sensitized
plate was 100 mg per cm^2 elevation exposure was obtained for
3-odd hours and the original. This study differences given
to a first approximation, the general resolution of the
photo-positive first derivative. The intensity of the electron
ionizes negative ions also affect on electrons and
photon penetrating energy. In order this effect, some
helium ions (photons) within them contained in the beam
and it was found that the spectrum-activity increased
decreased by $80 \pm 10\%$. This correlation was made on the
penetrating rays.

Before and after each run, electric bit counter was
calibrated as a function of various voltages (see figure 4).

Figure 4: Typical Calibration Curve

Figure 4 shows the calibration curve of bin number versus pulser volts. The limits of each bin is indicated by the short horizontal lines on either side of the bin number.

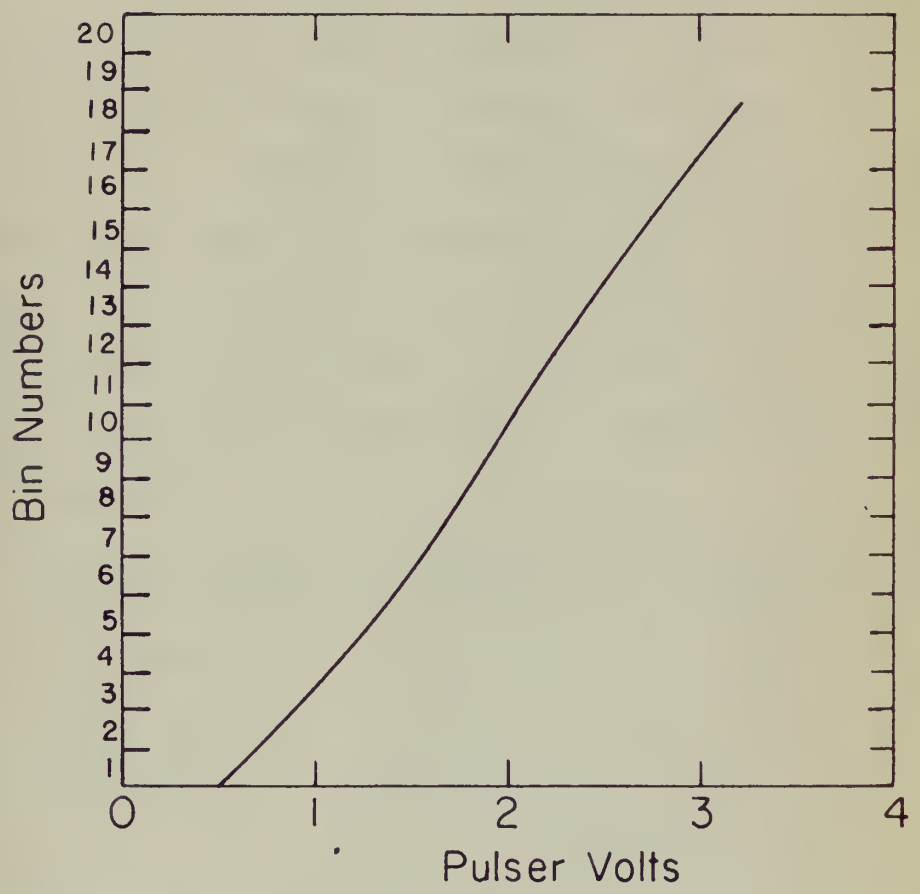

TYPICAL CALIBRATION CURVE

Figure 4

The data, recorded as counts per bin, was converted to counts per pulser volt. The counts per volt were plotted versus pulser volts for both the proton runs and the corrected background runs (see figures 5a, 5b, and 5c). The difference between the proton plus background and background curves was then plotted (see figure 6).

The proton energy loss corresponding to one pulser volt was estimated by comparing the maximum electron energy with an extrapolated maximum pulser voltage. The extrapolation is indicated by the dashed curve in figure 6 and is discussed in Appendix 1. The following results were obtained:

Run	Maximum electron or photon energy*	Maximum proton energy	Maximum pulser volts	Mev per pulser volt
I	11.5 Mev	4.63 Mev	2.05	2.26
II	13.75 Mev	5.76 Mev	2.55	2.27
III	15.5 Mev	6.63 Mev	2.9	2.29

Average $2.3 \pm .2$

The agreement in the last column is probably fortuitous because of poor statistics andthe arbitrary nature of the extrapolations involved in finding both the maximum electron energy and the maximum pulser voltage.

* The energy scale of the linear accelerator is known to about 5% using as a standard the $Cu^{63}(\gamma,n)Cu^{62}$ threshold at $10.61 \pm .05$ Mev (8).

The data, recorded as counts per min, was converted to counts per polar volt. The counts per volt were plotted versus polar volts (see figure 8a, 8b, and 8c). The difference between the inverse plus energized and deenergized curves was then plotted (see figure 8).

The peaks nearly line corresponding to one polar volt was estimated by comparing the maximum electron count with an extrapolated maximum polar voltage. The extrapolation is indicated by the dashed curve in figure 8 and is discussed in appendix I. The following results were obtained:

Run	Emitting electron orbital energy	Maximum photon energy	Maximum polar volts	Max per polar volt
I	12.5 Ryr	4.15 Ryr	3.05	3.38
II	24.70 Ryr	6.75 Ryr	5.85	3.87
III	36.5 Ryr	8.85 Ryr	8.8	3.80

Average 3.7 ± .2

The agreement to the ideal solution is probably fortuitous because of poor visibility making accurate reading of the extrapolated intercept in finding both the maximum electron energy and the maximum polar voltage.

A fine energy scale of the linear monochrometer is known to about 2% owing to a specified 10Å $Cu_{K\alpha}(1,3)Cu_{OK}$ linewidth at 19.01 ± .05 Ryr [17].

Figure 5a, 5b, 5c: Counts vs Pulser Volts

Background counts and background plus proton counts are plotted versus pulser volts.

Run I figure 5a

Run II figure 5b

Run III figure 5c

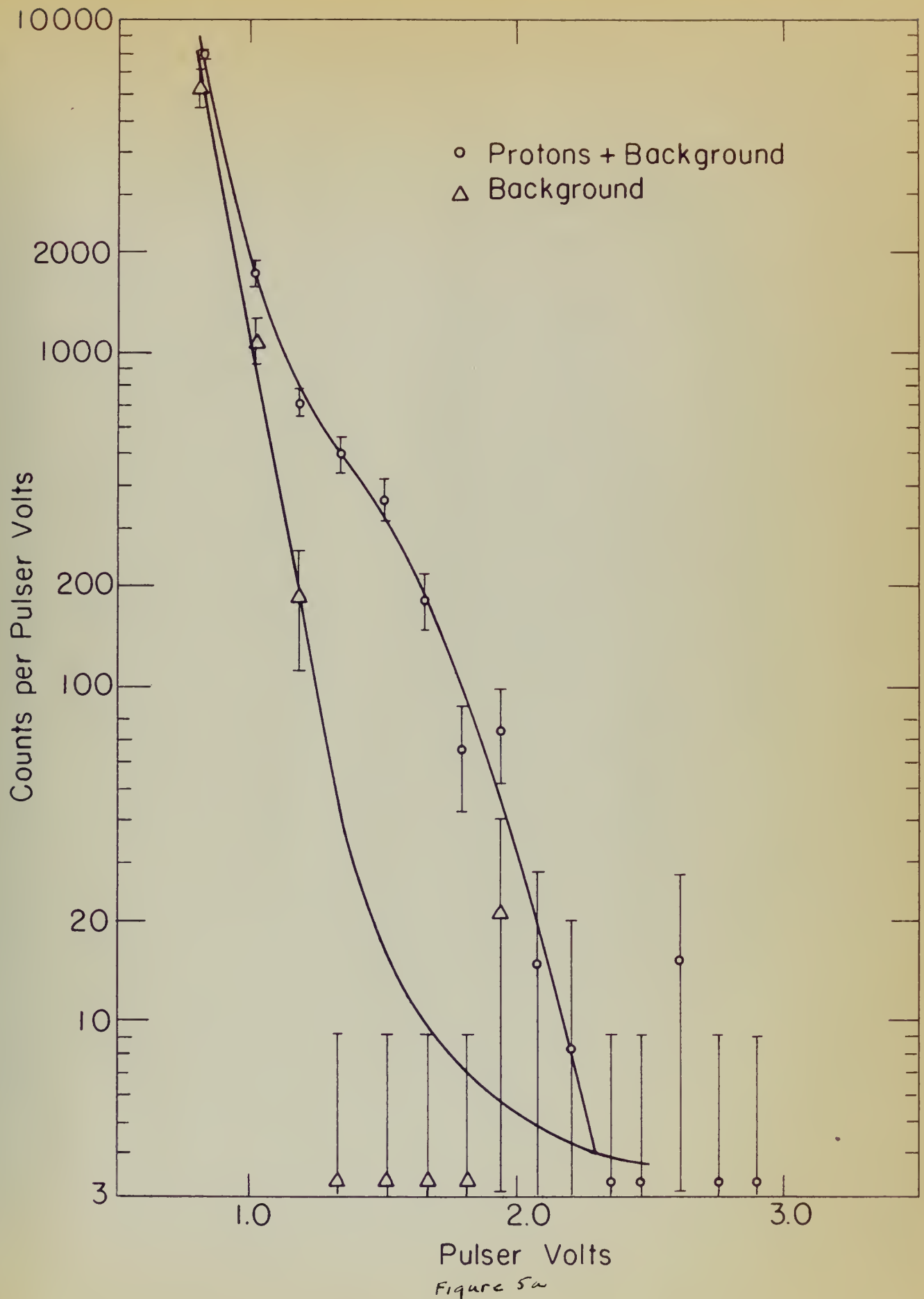
10000
2000
1000
200
100
20
10
3
Counts per Pulser Volts
Protons + Background
Background
1.0
2.0
3.0
Pulser Volts

Figure 5a

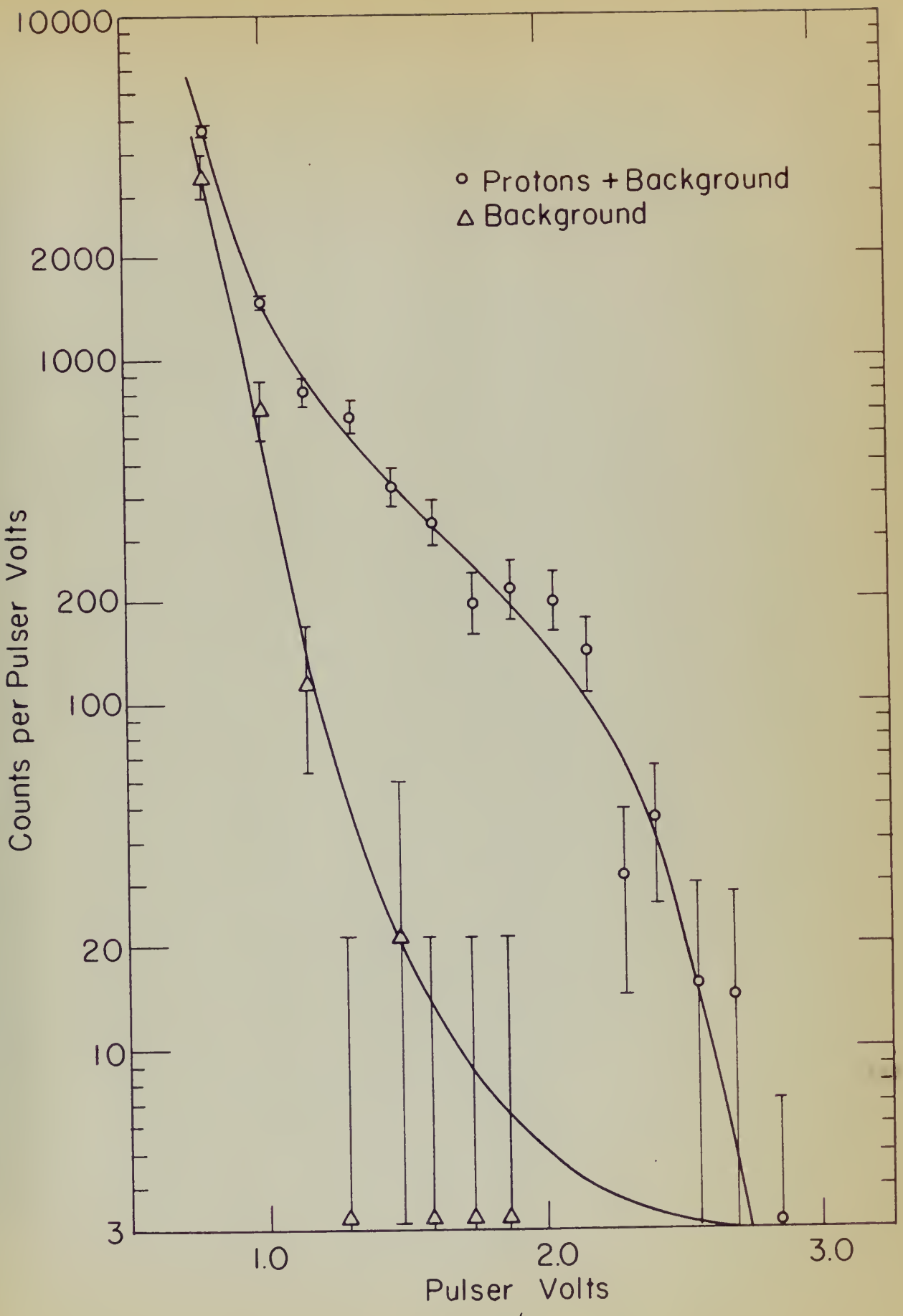
10000
2000
1000
200
100
20
10
3
Counts per Pulser Volts
o Protons + Background
Δ Background
1.0
2.0
3.0
Pulser Volts

Figure 5b

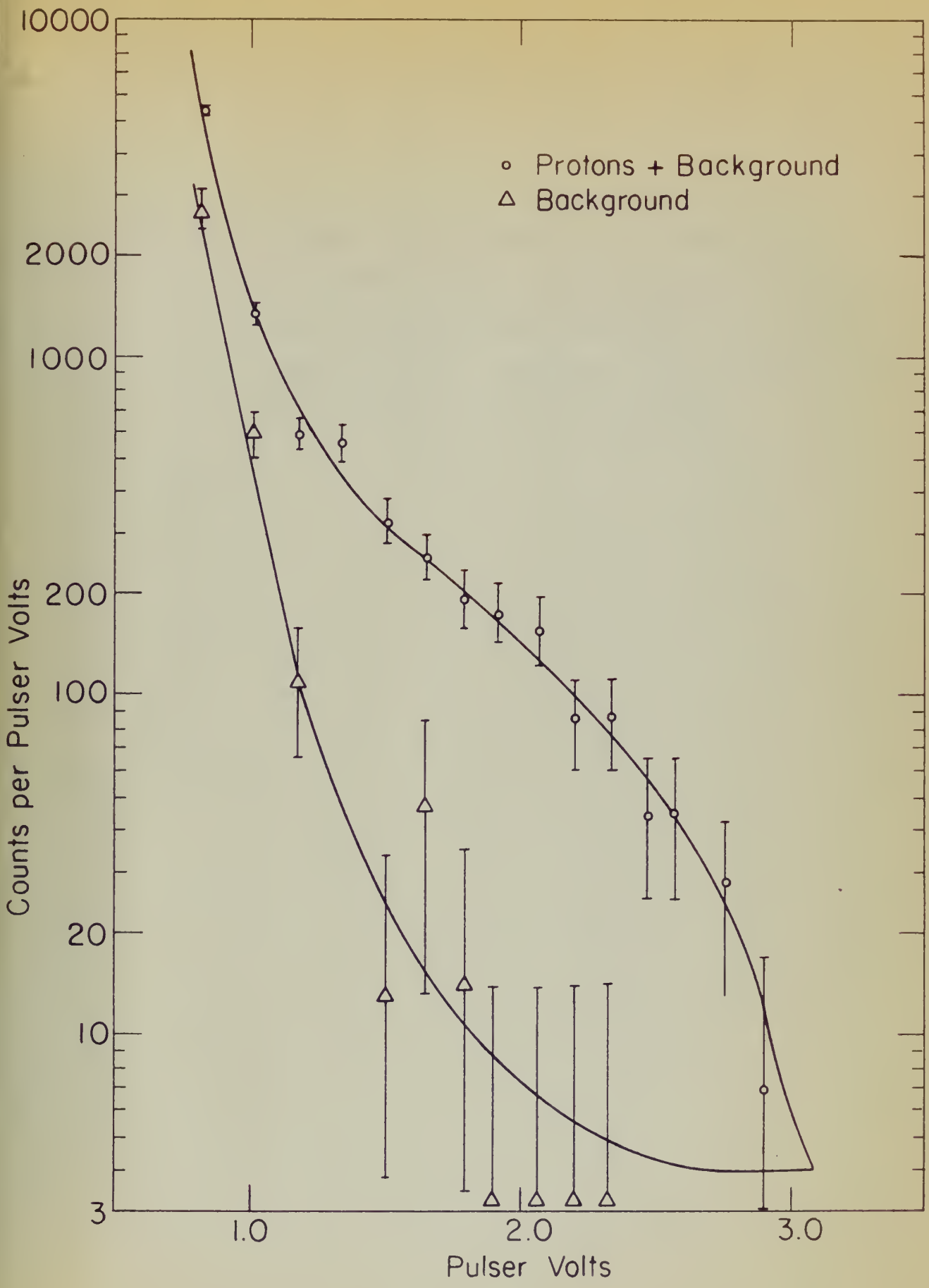
10000
2000
1000
200
100
20
10
3
Counts per Pulser Volts
Protons + Background
Background
1.0
2.0
3.0
Pulser Volts

Figure 5c

Figure 6: Proton Counts versus Pulser Volts

This figure shows the difference between proton plus background and background counts for run II. The dashed line indicates the extrapolation made to determine maximum pulser volts.

Figure 4a. Problem Domain Showing T-Wave Voltage

Data Figure showing the differences between proton plus beryllium and beryllium counts for run 11. The dashed line indicates the extrapolation made to determine maximum polar angle.

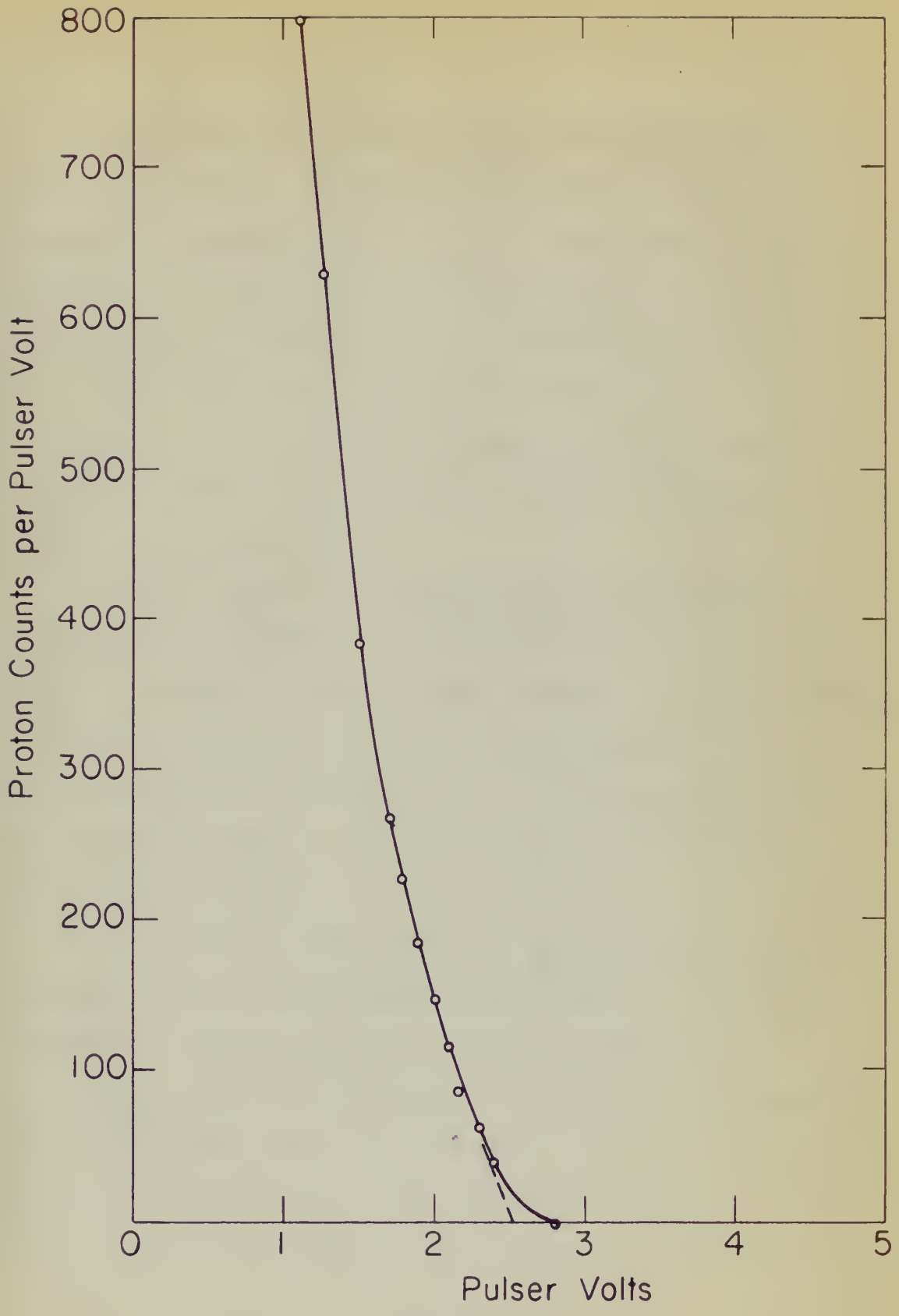
800
700
600
500
400
300
200
100
Proton Counts per Pulser Volt
0
1
2
3
4
5
Pulser Volts

Figure 6

During each proton run a 64 mg/cm^2 copper foil was in the X-ray beam. The activity induced in the foils provides more data for the energy calibration of the monitor. The information obtained from the Cu foils is discussed in appendix 2, and checks 2.3 proton Mev per pulser volt as the calibration constant.

Using the figure 2.3 Mev/pulser volt, the number of proton counts per volt can be converted to counts per mev of proton energy.

A curve of proton counts per mev of proton energy is drawn versus proton energy lost in the NaI(Tl) crystal. Such a curve is the dashed curve in figure 7. This spectrum must be corrected for the finite resolving power of the spectrometer and the energy loss of the proton in reaching the NaI(Tl) crystal, so that it becomes the spectrum of the photo-protons.

No correction, other than the extrapolation made above, in determining maximum pulser volts, is made for resolution. Resolution is discussed in appendix 1.

Energy is lost by a proton, in getting to the crystal, in the deuterium, and in the aluminum leaf over the crystal. An additional energy loss would occur if there were oil on the face of the crystal. This should be checked by

During each irradiation run a Cu mg/cm^2 copper foil was in the X-ray beam. The activity induced in the foils provides data for the energy calibration of the spectrometer. The information obtained from the Cu foils is discussed in appendix X, and assigns 8.9 protons per primary unit as its calibration constant.

Using the figure 8.9 Bev/primary unit, the number of proton events (n) will then be converted to counts per hour at proton energy.

A source of photon counts per hour of proton energy is known before proceed counts just in the Ba(II) crystal. Such a curve is the dashed curve in figure 7. This spectrum must be corrected for the finite resolving power of the spectrometer and the energy loss of the photon in passing the Ba(II) crystal, so that it becomes the expected form of the photo-photons.

To correction, curve down the assumptions made above, to unfortunately maximum photon yield, is made for truncation. Resolution is discussed in appendix I.

Energy is lost by a photon, in passing by the crystal, in the conversion, and by the alumimum leaf over the crystal. An additional energy loss occurs if light rays all on the face of the crystal. This should be checked by

using a monoenergetic γ-ray or proton source. In the absence of such information a correction has been made for a .25 mg/cm^2 oil film. In addition on the average the protons traverse 1.15 mg/cm^2 of deuterium and .27 mg/cm^2 of aluminum. The energy loss was calculated using the curves of M. Rich and R. Madey in U.C.R.L. 2304[9].

The corrected proton spectrum is drawn as a solid line in figure 7.

The simple approximation $h\upsilon = 2E_p + 2.23$ Mev was used to obtain photon energies from proton energies. For the actual geometry of the monitor the error in photon energy which comes from using this approximation is less than 1% over the entire 6-17 Mev range.

The differential cross section for d(γ,n)p as a function of laboratory angle is given by:

$$\sigma(\theta) = K(E)\left[a+\sin^2\theta\left(1+\left(\alpha+\frac{2\beta E}{E-W}\right)\cos\theta\right)\right] \quad (6)$$

where a and α are functions of the photon energy, E = photon energy, $\beta = \left(\frac{E-W}{M_p c^2}\right)^{\frac{1}{2}}$, and W is the binding energy of the deuteron.

using a monochromatic X-ray or proton source. In this
instance of wide-angle scattering a correction has been made
for a $\cos^2\theta$ polarization. In addition an ionization and
one photon fluorescence $\cos^2\theta$ at resonance and $\cos^4\theta$
at minimum. The weight loss was calculated
using the method of E. Gibb, and B. Hanley in W.C.R.I.
1974[9].

The commercial cross-section is based on a unity line
in Figure 7.

The atomic susceptibilities $\eta = 2\delta_0 + 8.4\beta$ has been used
to obtain phonon modulation from previous examples. For the
actual geometry of the machine the mirror in double reflect
mode causes line width broadening in less than 1%
case the matrix 8-12 Day Model.

The differential cross section $\frac{d(\lambda,\eta)\rho}{}$ as a
function of polarization angle is given by:

$$\sigma(\theta) = K\lim\left[\frac{1+\alpha\eta_0^2\theta}{}\right](\gamma+(\alpha+\frac{1}{2}\beta)\cos\theta)(\theta)$$

where α and $\alpha\alpha$ functions of the photon energy. $M =$
photon energy, $\theta =$ $\left(\frac{}{}\right)$. and M is the binding energy of
the neutrons.

The following values were used:

E	a	$\alpha + \frac{2\beta E}{E-W}$
7	.05	.34
9	0	.39
11	.1	.43
13	.2	.46
15	.2	.50

K(E) is determined from the total cross section curve drawn by J. S. Levinger [4], (see figure 8). For the energy region of interest the Lovinger curve is based primarily on the data of Barnes, Carver, Stafford and Wilkinson [1].

The number of proton counts per Mev for a given photon energy is given by $N(E) = \int \Omega(x) \phi(E) N_d \sigma(x,E) dx = \phi(E) Y(E)$ where the integration is carried out over that portion of the photon beam seen by the NaI(Tl) crystal. N(E) = total number of proton counts per Mev at the desired photon energy, $\phi(E)$ = the number of photons per Mev at that energy, N_d = number of deuterium atoms per cm^3, and Ω = the solid angle subtended by the crystal. The effective efficiency Y(E) is tabulated for several photon energies:

E	6	7	8	9	10
Y(E)	2.50×10^{-9}	2.29×10^{-9}	2.05×10^{-9}	1.80×10^{-9}	1.55×10^{-9}

11	12	13	14	15	16
1.32×10^{-9}	1.20×10^{-9}	1.10×10^{-9}	$.98 \times 10^{-9}$	$.91 \times 10^{-9}$	$.85 \times 10^{-9}$

The photon spectrums for runs I, II, and III are shown in figures 9a and 9b. The vertical bars on the curves indicate the order of magnitude of the statistical and background uncertainties.

The insert in figures 9b is an estimate of the electron spectrum for run II. The spectrum is measured by magnetic deflection of the electron beam. Because of the quadrapole focusing coils this spectrum, however, may not be the spectrum of the beam at the X-ray target, also the spectrum shifts somewhat in energy and intensity during a run. The electron spectrum shown is an average of the before run and after run spectrums.

From this estimated spectrum a thin target bremsstrahlung curve was calculated and is shown by the dashed curve in figures 9b. This curve was obtained using Bethe-Heitler bremsstrahlung tables prepared by the MIT linear accelerator group. Although the lead x-ray target was 0.3 cm thick, one might expect only the first hundredth of a radiation length to contribute appreciably to the bramsstrahlung intensity in the forward direction. A 10 Mev electron is scattered through an rms. angle equal to $\frac{mc^2}{E}$ in less than 10^{-3} radiation lengths. The thin target curve was normalized to the experimental curve at 10 Mev. This normalization corresponds to an effective X-ray target thickness of only about 2×10^{-3}

radiation lengths (10^{-3}cm.) if one believes that with the strong focusing coils, the collimator sees the entire electron current.

radiation lengths (10^{-2} cm.) if the material used was the strong focusing coils, the collimator near the active electron beams.

Figure 7: Protons per Mev versus Proton Energy for Run II
The dashed curve indicates the experimental results before correction for slowing down of the protons in deuterium, aluminum, and oil. The solid curve is the corrected protons versus proton energy curve.

Figure 11: Problems per Day Versus Typing Speed for Draft
The dashed curve indicates the experimental
results before correction for slowing down of
the problems in destructive, aluminum, and oil.
The solid curve is the compressed previous curve
shifted upward.

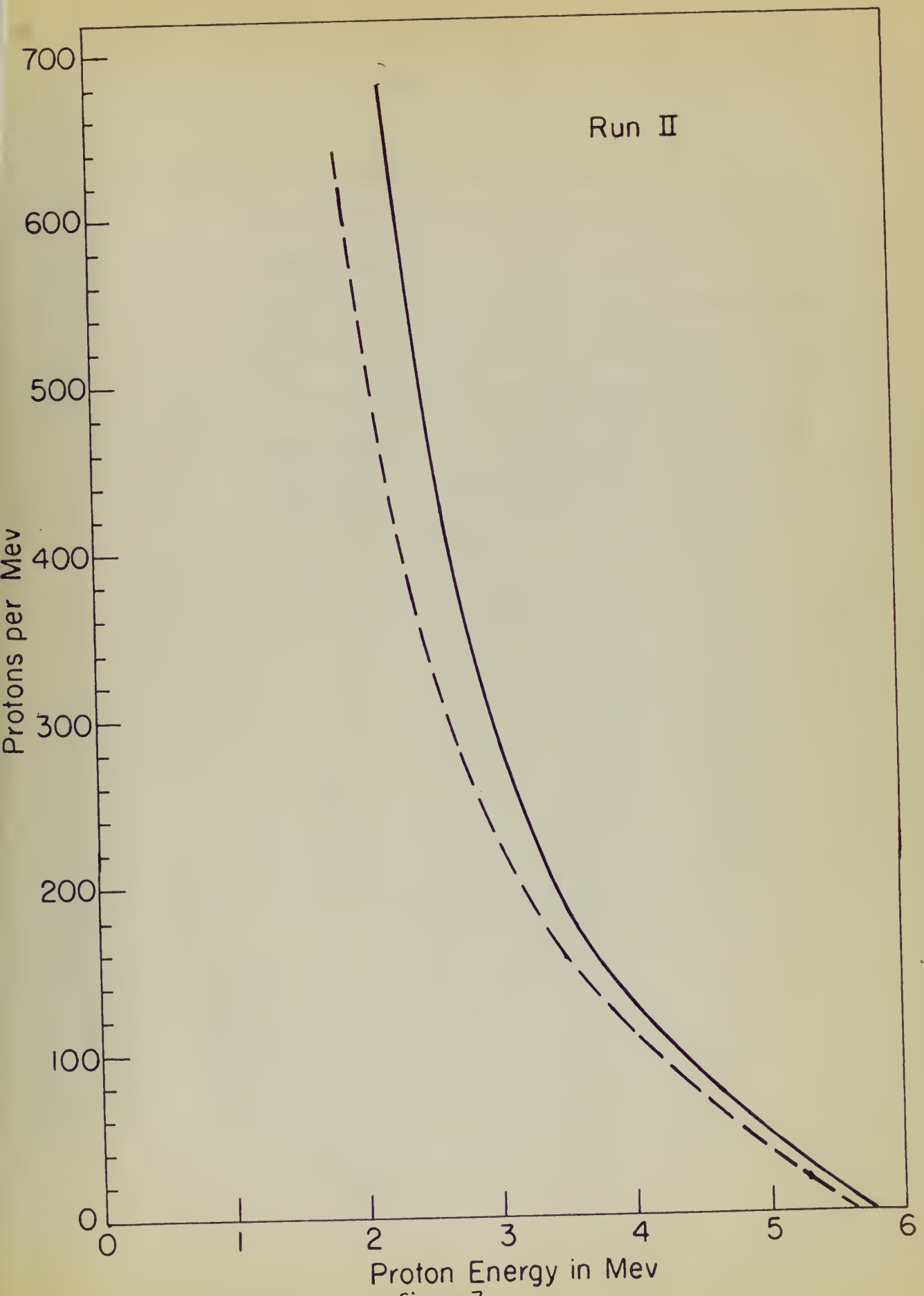
Run II
700
600
500
400
300
200
100
0
Protons per Mev
0
1
2
3
4
5
6
Proton Energy in Mev

Figure 7

Figure 8: Cross section curve for d(,n)p
This cross section curve is taken from the curve drawn by J. S. Levinger [4]. The points labeled are the experimental values of the cross section as determined by Barnes, Carver, Stafford, and Wilkinson [1]. The point labeled is the experimental value obtained by J. Halpern and B. V. Weinstock.[2]

Figure 8: Cross section curve for dl .mip

This curve section curve is taken from the curve given by J. S. Lavinger [4]. The points labeled are the experimental values of the curve sections as determined by Barnes, Culver, Bradford, and Wilkinson [1]. The polar labeled is the experimental value obtained by J. Halpern and R. V. Waterston.[3]

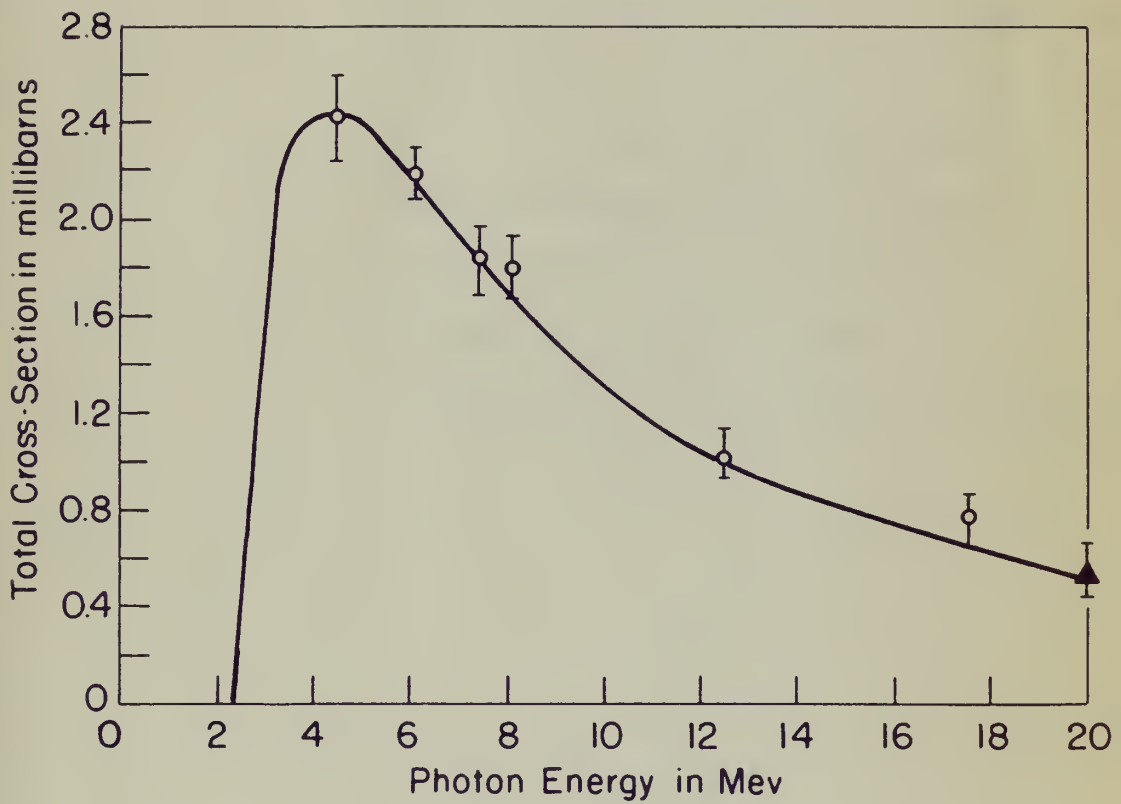
Total Cross-Section in millibarns
2.8
2.4
2.0
1.6
1.2
0.8
0.4
0
0
2
4
6
8
10
12
14
16
18
20
Photon Energy in Mev

Figure 8

Figure 9a, 9b, [illegible]: Photons per Mev versus Photon Energy
Figure 9a is the result of run I and run III, and figure 9b is the result of run II. On figure 9b is an insert showing the electron spectrum for run II in micro amperes per Mev versus electron energy. The dashed curve in figure 9b is the calculated thin target bremsstrahlung spectrum for run II. The vertical bars on the curves in figures 9a and 9b indicate the statistical and background uncertainities.

Figure 9a, 9b. : Positions per day versus Fluton Number
Figure 9a is the result for run I and
run III, and Figure 9b is the result
of run II. On Figure 9b is an insert
showing the elevations experienced for run
II in which emphasis was put upon
time control. The dashed curve in Figure
9b is the calculated tide having
parameters specified for run II.
The vertical bars on the curves in
Figures 9a and 9b indicate the
statistical and background uncertainties.

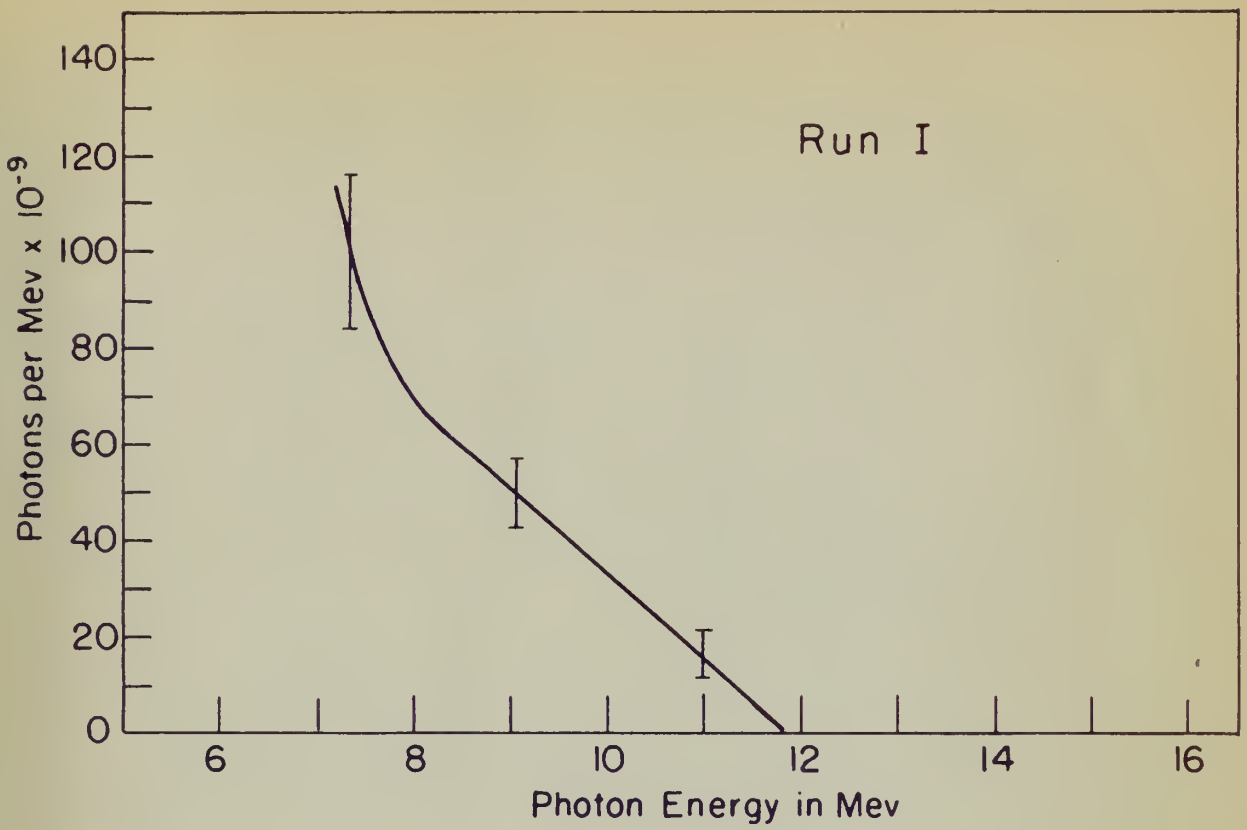
Run I
Photons per Mev x 10^{-9}
140
120
100
80
60
40
20
0
6
8
10
12
14
16
Photon Energy in Mev

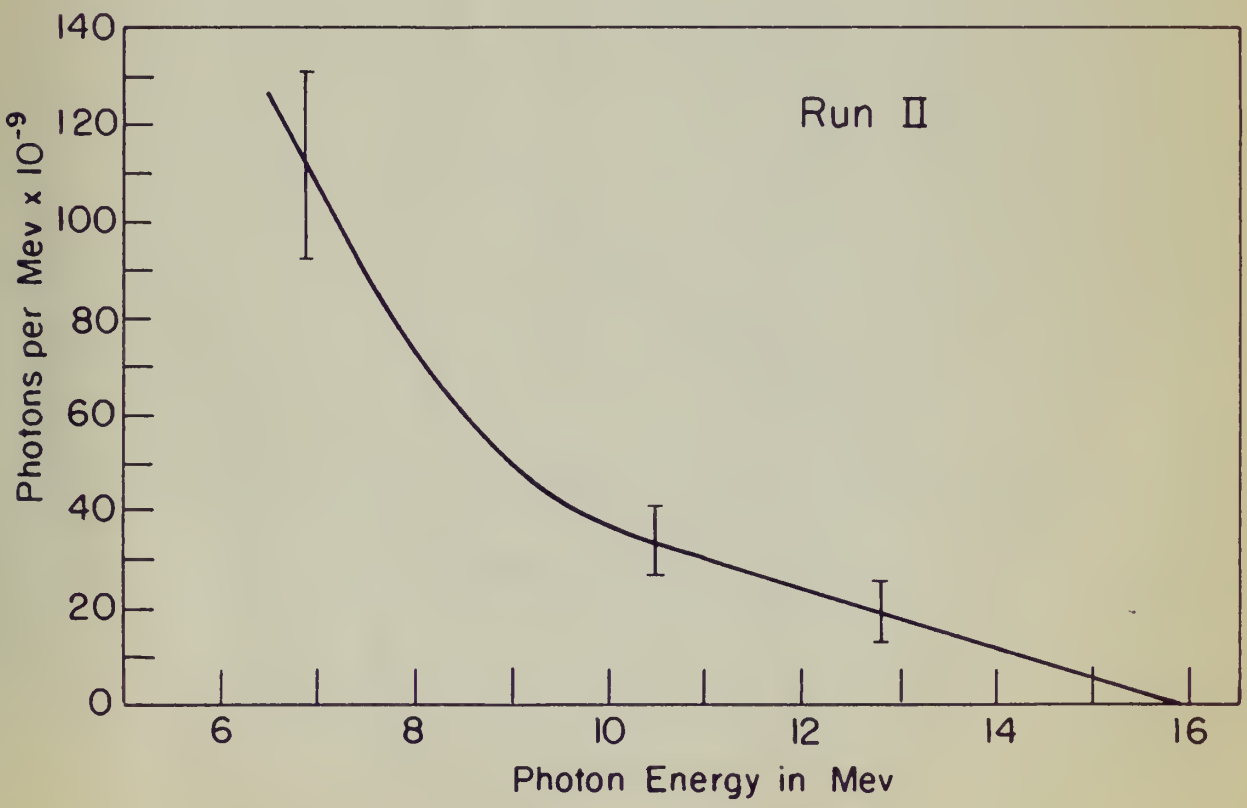
Run II
Photons per Mev x 10^{-9}
140
120
100
80
60
40
20
0
6
8
10
12
14
16
Photon Energy in Mev

Figure 9a

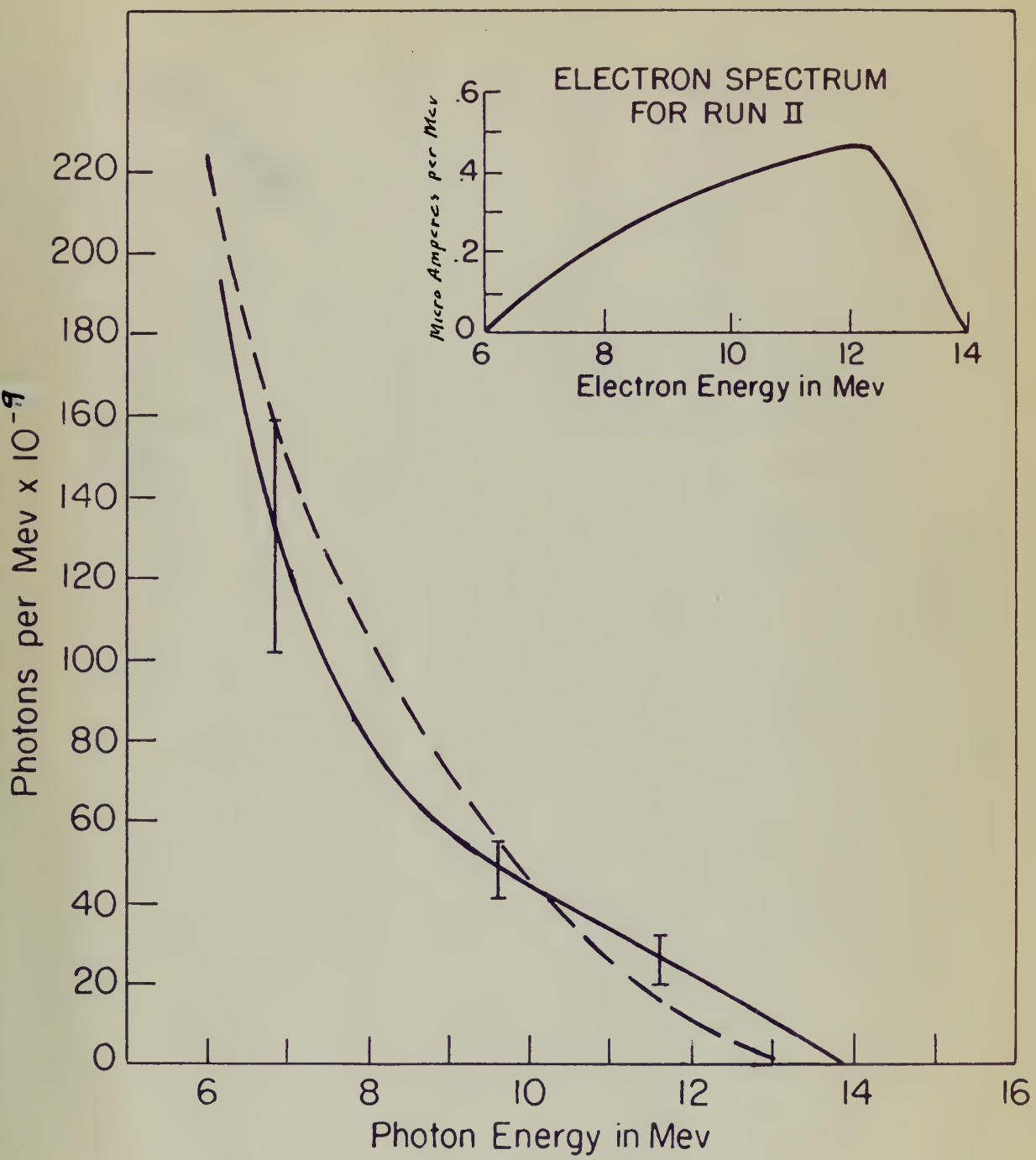
ELECTRON SPECTRUM
FOR RUN II
Micro Amperes per Mev
.6
.4
.2
0
6
8
10
12
14
Electron Energy in Mev
Photons per Mev x 10^{-9}
220
200
180
160
140
120
100
80
60
40
20
0
6
8
10
12
14
16
Photon Energy in Mev

Figure 9b

VI Conclusions

An X-ray spectrometer designed to monitor the bremsstrahlung beam of the linear accelerator, and based on the d(γ,n)p cross section has been tested. In addition to adequate energy resolution a suitable monitor must be efficient, in that its statistics must be better than the statistics of the experiment monitored. The present monitor satisfies this requirement only for experiments with rather low counting rates, and which measure cross sections which are not particularly sensitive to the exact shape of the incident photon spectrum.

Some conversions should be made to make the monitor more adaptable. A smaller chamber should be constructed which can be pressurized, allowing for a variation in the amount of deuterium. For experiments where only the upper end of the photon spectrum is required or where shorter runs will be made, a higher pressure could be used to advantage. For long runs and for experiments where the photon spectrum from 6 Mev up is desired, atmospheric pressure should be used to minimize corrections for energy loss in the deuterium.

VI Conclusions

APPENDIX I

Resolution

Energy resolution of protons may be affected by pile up of pulses in the crystal, radio frequency pick up from the linear accelerator, photomultiplier statistics, and the geometry of the monitor.

The effect of pile up was neglible. There was less than one (usually small) pulse in the crystal during one micro-second accelerator burst. The pulses from the crystal were clipped to .15 micro-seconds.

Radio frequency pick up was also neglible.

The effect on resolution of the statistical nature of energy detection in the crystal and the photo multiplier was calculated assuming 300 photo electrons at the first photo multiplier dynode per Mev of proton energy lost in the crystal. The full widths at half maximum of the Gaussian resolution functions resulting from photomultiplier statistics are tabulated for photon energies of 7, 11, and 15 Mev in the table on page 27.

The lack of resolution which results from the geometry of the monitor comes from two effects. The first effect is that protons, originating from different parts of the X-ray beam seen by the crystal, travel different path lengths before reaching the crystal. Therefore some protons

APPENDIX I

Resolution

Energy resolutions of systems may be affected by pile up of pulses in the crystal, radio frequency pick up from the linear accelerator, photomultiplier statistics, and the geometry of the monitor.

The effect of pile up was negligible. There was less than one (usually small) pulse in the crystal during one micro-second accelerator burst. The pulses from the crystal were clipped to .15 micro-seconds.

Radio frequency pick up was also negligible.

The effect on resolution of the statistical nature of energy deposition in the crystal and the photo multiplier was calculated assuming 300 photo electrons at the first photo multiplier dynode per Mev of proton energy lost in the crystal. The full widths at half maximum of the Gaussian resolution functions resulting from photomultiplier statistics are tabulated for photon energies of 7, 11 and 15 Mev in the table on page 27.

The lack of resolution which results from the geometry of the monitor comes from two effects. The first effect is that protons, originating from different parts of the X-ray beam enter by the crystal, travel different path lengths before reaching the crystal. Therefore some protons

will lose more energy in the deuterium than others. This effect is small, amounting at most to about a .5% energy uncertainity at 2 Mev and .3% at 3 Mev. This effect was neglected and the curves of protons per Mev versus proton energy were corrected for an average path length in the deuterium.

The second effect comes from the finite momentum of the incident photon. From conservation laws the photon energy can be shown to be: (7)

$$h\upsilon = \frac{1875.3T_p + 2099.0}{937.18 - T_p + (1876.2T_p + T_p^2)^{\frac{1}{2}}\cos\theta}$$

The same proton energy, as measured by the monitor, corresponds to various values of $h\upsilon$ depending upon θ

The minimum angle seen by the crystal is 55° and the maximum 125°. The following table shows the effect of angle on $h\upsilon$ for various proton energies:

T_p	$h\upsilon$ at θ = 90°	75°	105°	55°	135°
1	4.24	4.2	4.29	4.13	4.37
2	6.26	6.15	6.36	6.03	6.50
3	8.28	8.1	8.45	7.91	8.67
4	10.30	10.1	10.51	9.77	10.88
5	12.32	12.0	12.65	13.10	11.62
6	14.34	13.93	14.79	13.47	15.33
7	16.35	15.84	16.9	15.32	17.47

The resolution due to geometry is calculated using differential cross section and solid angle weighted values

will lose more energy in the deuterium than others. This effect is small, amounting at most to about a .3% correction at 2 Mev and .5% at 3 Mev. This effect was neglected and the curves of neutron per Mev versus proton energy were corrected for an average path length in the deuterium.

The second effect comes from the finite resolution of the incident proton. From conservation laws the proton energy can be shown to be: (7)

$$h\nu = \frac{187.7T_p^2 + 2000.0}{387.7\theta - T_p^2 + (187.7T_p^2 + T_p^2)\cos\theta}$$

The same proton energy, as measured by the monitor, corresponds to various values of $h\nu$ depending upon θ. The stated angle read by the crystal is 55° and its maximum 125°. The following table shows the effect of angle on $h\nu$ for various proton energies.

T_p $h\nu$ at θ =	90°	75°	105°	55°	125°
2	4.34	4.3	4.39	4.13	4.37
3	6.04	6.15	6.46	6.05	6.30
4	7.80	8.1	8.43	7.81	8.07
5	10.00	10.1	10.01	9.77	10.25
6	12.25	12.0	12.65	12.10	11.69
7	14.24	13.03	14.78	13.47	15.55
	16.56	15.54	16.9	15.35	17.47

The resolution due to geometry is calculated using differential cross section and solid angle weighted values

for different angles and is included in the following table.

Full width at half maximum of the resolution functions

hν	Photo Multiplier	Geometry	Total
7	8%	7.0%	11%
11	5.5%	9.5%	11%
15	4.5%	10.6%	12%

To find the true number of protons per pulser volt from the measured number of protons per pulser volt we assumed a Gaussian resolution function:

1) $$F(E_0) = \frac{1}{\sqrt{2\pi}\,\sigma} \int_{-\infty}^{\infty} F_1(E)\, e^{-\frac{(E-E_0)^2}{2\sigma^2}}\, dE$$

where $F(E_0)$ = true number of protons per pulser volt at E_0, $F_1(E)$ = measured number of protons per pulser volt at E_0, σ is the half width of the Gaussian resolution function.

Assuming that $F(E_0)$ is a smooth function of E_0, an adequate approximation to 1 is:

$$F(E_0) = F_1(E_0) + \frac{\sigma^2 F_1''(E_0)}{2}$$

where $F_1''(E_0)$ is the second derivative of F_1 with respect to pulser volts evaluated at E_0. For example, in Run II the maximum second derivative for the curve is about 2000 counts per volt^3 at 1.5 pulser volts, and the correction $F(1.5)-F_1(1.5)$ is $\frac{(.055)^2(2000)}{2}$ = 3 counts in 300 or 1%.

for different angles and is included in the following table.

Unit weight at half maximum of the resolution functions

	Energy	Multiplier	Quantity	Total
	15	4.5%	10.0%	12%
	11	8.5%	6.3%	11%
	0	0%	7.0%	11%

To find the true number of protons per pulser volt

then the measured number of protons per pulser volt as

assumed a Gaussian resolution function:

$$1) \quad F(\varepsilon') = \frac{1}{\sigma\sqrt{2\pi}} \int_{-\infty}^{\infty} F(\varepsilon)\, e^{-\frac{(\varepsilon-\varepsilon')^2}{2\sigma^2}}\, d\varepsilon$$

where $N(E^0)$ = true number of protons per pulser volt at E^0, $N'(E)$ = measured number of protons per pulser volt at E^0, σ is the half width of the Gaussian resolution function.

Assume that $N(E^0)$ is a smooth function of E^0, an adequate approximation to 1 is:

$$N(E^0) = N'(E^0) + \frac{\sigma^2}{2} N''(E^0)$$

where $N''(E^0)$ is the second derivative of N' with respect to pulser volts evaluated at E^0. For example, in run II the maximum second derivative for the curve is about 8000 counts per pulser volt^2 at 3.0 pulser volts, and the correction

$N(E)-N'(E)$ is $\frac{(.05)^2(8000)}{2}$ = 2 counts in 200 or 1%.

This correction for resolution was neglected except that the "tail" of the curve was corrected by the extrapolation of the protons per pulser volt curve as shown in Figure 6.

This correction for resolution was neglected except that the "tail" of the curve was corrected by the extrapolation of the crosses per number unit curve as shown in Figure 6.

APPENDIX II

The cross section of the $Cu^{63}(\gamma,n)Cu^{62}$ reaction at 12 Mev.

The $Cu^{63}(\gamma,n)Cu^{62}$ reaction is a particularly easy photon nuclear reaction to study. The unstable Cu^{62} decays almost entirely by positron emission with a maximum positron energy of 2.9 Mev and a convenient 9.7 minute half life. The high positron energy makes it possible to measure the induced radioactivity with considerable confidence.

Most of the $Cu^{63}(\gamma,n)Cu^{62}$ cross section measurements have been dependent upon the calculated response of ionization meters. However, Krohn and Shrader have used a pair spectrometer calibrated against the cross section for the photodisentegration of the deuteron to monitor the X-ray flux(15). The most precise absolute measurement is that of Berman and Brown (14) who used an integrated electron current measurement and the Bethe-Heitler bremsstrahlung cross section to obtain the photon flux.

Berman and Brown find that the $Cu^{63}(\gamma,n)Cu^{62}$ cross section rises from the threshold at 10.61 Mev to a value of 21 mb. at 13 Mev and continues to rise up to a giant resonance peak of 98 mb. at 17.7 Mev. The absolute precision is better than 10%.

APPENDIX II

The cross section of the $Cu^{63}(\gamma,n)Cu^{62}$ reaction at 13 Mev.

The $Cu^{65}(\gamma,n)Cu^{64}$ reaction is a particularly easy photon neutron reaction to study. The neutrons Cu^{64} decays almost entirely by positron emission with a maximum positron energy of 0.6 Mev and a corresponding 6.7 minute half life. The high positron energy makes it possible to measure the induced radioactivity with considerable confidence.

Most of the $Cu^{65}(\gamma,n)Cu^{64}$ cross section measurements have been dependent upon the neutron sensitive reactions of ionization meters. However, Bothe and Gentner have used a pair spectrometer calibrated against the cross section for the photodisintegration of the deuteron to measure the X-ray flux(18). The most trustworthy absolute measurement is that of Bothe and Gentner (14) who used an integrated electron current measurement and the Bothe-Geitler triple coincidence method to obtain the photon flux.

Baldwin and Brown find that the $Cu^{63}(\gamma,n)Cu^{62}$ cross section rises from Ore Cumberland at 10.2 Mev to a value of 21 mb. at 13 Mev and continues to rise up to a giant resonance peak of 58 mb. at 17.7 Mev. The absolute precision is better than 10%.

Although the precision will not be comparable to that of Berman and Brown's experiment, it is interesting to use the test curves of the X-ray monitor to measure the Cu^{63} cross section in the 11 to 15 Mev region.

During each one hour run a 64 mg/cm^2 natural copper foil was exposed at the end of the X-ray collimator. After the run the foil activity was counted in a 2π geometry with an end window Geiger tube. From the decay curve the counting rate, R, at beam off time due to the 10 minute Cu^{62} activity was determined. Since the exposure time was more than six times the half life of Cu^{62}, the total yield is very nearly:

1) $$Y = 2Rt\ 1.12$$

where Y is total activated nuclei in the foil corresponding to $Cu^{63}(\gamma,n,)Cu^{62}$ and t is the exposure time (1 hour). The factor 2 comes from the 2π counter geometry, and the 1.12 represents a 12% correction for self absorbtion of the positions in the foil.(16) No correction for back scattering in a thick brass foil holder is necessary. This was checked by simultaneously activating the standard foil and a thick foil (730 mg/cm^2). The corrected counting rates agree within the 3% statistics. No correction is made for electron capture. The decay scheme for Cu^{62} is not yet

Although the precision will not be comparable to that of Jensen and Brown's experiment, it is important to see the test curves of the 1-cap position to measure the Cu^{62} cross section in the 12 Mev region.

During each run, two 0.05 gm/cm^2 natural copper foil was exposed at the end of the 1-cap collimator. After the run the foil activity was counted in a 2π geometry with an end window Geiger tube. From the decay curve the counting rate, R, at zero off time due to the 10 minute Cu^{62} activity was determined. Since the exposure time was more than six times the half life of Cu^{62}, the total yield is very nearly:

1) $\quad X = 2.88\ I.R$

where X is total activated nuclei in the foil corresponding to $Cu^{62}(\gamma,n')Cu^{62}$ and I is the exposure time (1 hour). The factor 2 comes from the 2π counter geometry, and the 1.12 represents a 10% correction for foil absorption of the positrons in the foil.(10) No correction for back scattering in a thick brass foil holder is necessary. This was checked by alternately matching the standard foil and a thick foil (720 gm/cm^2). The corrected resulting rates were within the 3% reliable. No correction is made for electron capture. The decay scheme for Cu^{62} is not yet

known in detail, but the electron capture to positron emmission ratio is probably not more than a few percent.

The measurement of Y by (1) assumes that the X-ray intensity and spectrum remains constant during the run. For run I and run II the intensity as monitored by the Beckman ionization chamber was essentially constant and the electron spectrum measured after the runs checked well with the spectrum measured before the runs. Run III however was useless as a measurement of the $Cu^{63}(\gamma,n)Cu^{62}$ cross section.

The yield is related to the reaction cross section $\sigma(E)$ by

$$Y = N\int_{E_t}^{E_{max}} \sigma(E)\phi(E)dE \qquad (2)$$

where N is the number of Cu^{63} nuclei per cm^2, E is the quantum energy in Mev, and ϕ is the total number of photons per Mev passing through the foil. ϕ is measured by the monitor.

The measured photon spectra are, within the poor statistics, essentially linear between the reaction threshold, E_t = 10.61 Mev, and the maximum photon energy E_{max}. If we take $\phi(E) = B(E_M - E)$, and further, approximate the reaction cross section by a straight line rising from threshold $\sigma(E) = K(E-E_t)$ equation (2) becomes

$$\sigma(E)\,dE$$

$$I = N \int_{E'}^{E_{max}} \sigma(E)\phi(E)\,dE$$

where I is the number of Cu^{65} nuclei per cm^2, N is the quantity measured in Exp., and ϕ is the total number of neutrons per Exp passing through the foil. ϕ is measured by the monitor.

The measured cross sections are, within the probable errors, essentially linear between the threshold curves. If we take $\phi(x) = Ae^{-Bx}$, and further, approximate the integral $\sigma(E)\,dE = K(E-E')$ equation (3) becomes

Boston Public Library

3) $$Y = \frac{NKB}{6}(E_m - E_t)^3$$

The total yield from run II (the sum of the two one hour runs) is Y = $8.2 \times 10^4 \pm 5\%$. From figure 9b, E maximum = 13.85 Mev and B = 12×10^9 Mev $^{-2}$. From (3) K = 3.5×10^{-27} cm^2 per Mev.

At 12 Mev the $Cu^{63}(\gamma,n)Cu^{62}$ cross section is then calculated to be 5 mb.

A more precise measurement of $\phi(E)$ near E maximum would probably reveal a positive second derivative (compare the calculated thin target spectrum in figure 9b) which would tend to increase the measured value of the cross section.

Also, in Run II, the maximum electron energy of the acceleration did decrease by about .5 Mev during the run. The E maximum measured by the monitor, which monitors the X-ray beam the entire run, is probably higher than the E maximum responsible for the Cu activity. This difference in electron energy would also tend to increase the measured value of the cross section. At worst, if a .6 Mev decrease in maximum electron energy occurs about 15 minutes before the end of a run the measured cross section would be about 10 mb. at 12 Mev. An extrapolation of the Berman and Brown cross section yields about 9 mb. at 12 Mev.

$$\int_0^{E_{max}} \frac{\sigma(E)}{(E_{max}-E)^{\frac{1}{2}}} \, dE$$

The total yield from eq 11 (the sum of the two one hour runs) is $Y = 0.8 \times 10^{-2} \pm 3\%$. From figure 9b, Φ maximum = 12.85 Mev and $\Phi = 12 \times 10^{13} \text{ Mev}^{-2}$. From (3) $\varepsilon = 3.8 \times 10^{-27} \text{cm}^2$ per Mev.

At 12 Mev the $Cu^{63}(\gamma,n)Cu^{62}$ cross section is then calculated to be 6 mb.

A more precise measurement of $\Phi(E)$ near E maximum would probably reveal a positive second derivative (compare the calculated thin target spectrum in figure 9b) which would tend to increase the measured value of the cross section.

Also, in Run II, the maximum electron energy of the accelerator was determined by about .3 Mev during the run. The Φ maximum measured by the monitors, which monitors the X-ray beam (the entire run, in probably higher than the E maximum responsible for the Cu activity. This difference in electron energy would also tend to increase the measured value of the cross section. As above, if a .3 Mev decrease in maximum electron energy occurs about 12 Mev, eq 11 changes by the end of a run the measured cross section would be above by 4%. As it was, no correction of this between and Brooks cross section yields above 3 mb, as it was.

For run I Y = 1.2×10^4, E_{max} = 11.9 Mev, and B = 18×10^9 Mev $^{-2}$ giving K = 4.5×10^{-27} $cm.^2$ per Mev.

E_{max} is, however, so close to E_t that the data is useful only as a check on the energy calibration of the monitor. A 5% change in the calibration constant (2.3 proton Mev per pulser volt) would change the measured K by about a factor of 4. The Cr^{52} yield from run I then provides evidence that the energy calibration is probably correct 5%.

For run I = 1.58$10^{4}$, E_{max} = 11.6 Bev, and R = 1860σ

use σ fission E = 6.1 $\times 10^{-27}$ cm^2 per Bev.

E_{max} is, however, so close to E_t that the data is useful only as a check on the energy calibration of the monitor. A 5% change in the calibration constant

(8.5 Bevatrons Bev per Faraday volt) would change the measured E by about a factor of 4. The C^{12} plate from run I probably contains 8%.

does provides evidence that the energy calibration is

REFERENCES

1. Barnes, Carver, Stafford, and Wilkinson, Phys. Rev. 86, 359 (1952)

2. J. Halpern and E. V. Weinstock, Phys. Rev. 91, 934 (1953)

3. Marian, Bishop, and Halban, Proc. Phys. Soc. (London) A67,1113 (1954)

4. J. S. Levinger, Phys. Rev. 97, 971 (1955)

5. J. C. Noyes, J. E. Van Hoomissen, W. C. Miller, B. Waldman, Phys. Rev. 95, 396, (1954)

6. E. G. Fuller, Phys. Rev. 79, 303 (1950)

7. Circ. Nat. Bur. Stand. #515 (1951)

8. A. M. Birnbaum, Phys. Rev 93, 146, (1954)

9. M. Rich and R. Madey UCRL 2301 (1954)

10. V. E. Krohn and E. P. Schrader, Phys. Rev. 86, 391, (1952)

11. K. Phillips, Phil. Mag. 43, 129 (Jan. 1952)

12. E. Segre, Experimental Nuclear Physics, Vol. I

13. Bethe-Heitler Bremsstrahlung Table prepared by MIT linear accelerator group

14. A. I. Berman and K. L. Brown, Phys. Rev. 96, 83 (1954)

15. V. E. Krohn and E. P. Schrader, Phys. Rev. 87, 685 (1952)

16. R. G. Baker and L. Katz, Nucleonics, 11, No.2 14 (1953)

1. Bureau, Garvey, Shelford, and Wilkinson, Phys.
Rev. 69, 580 (1946)

4. J. Halpern and S. V. Peinstone, Phys. Rev. 91,
954 (1953)

3. Martin, Shapley, and Wallace, Phys. Soc.
(London) A67,1113 (1954)

4. V. S. Levinger, Phys. Rev. 97, 423(1955)

5. J. C. Noyes, J. E. Van Boomtaamm, W. C. Miller,
S. Weinbaum, Phys. Rev. 98, 886, (1954)

6. E. M. Brolley, Phys. Rev. 74, 303 (1950)

7. Clro. Rel. Expr. Manc. 2019 (1953)

8. A. E. Stephens, Phys.Rev. 93, 136, (1954)

9. W. Allen and E. Hanby NRDC N302 (1954)

10. V. F. Cowan and E. F. Hinterman, Phys. Rev. 82,
801, (1950)

12. K. Phillips, Proc. Camp. Ac, 128 (Jan. 1958)

13. E. Segre, Experimental Nuclear Physics, Vol. I

15. Bethe-Hoffler Penetration Table prepared by
Cll Linac Modulator Group

14. A. I. Burgad and E. L. Brown, Rdgs. Rev. 90, 83 (1954)

15. V. L. Fowler and K. V. Vaidyanathan, Proc. Rev. 87,
886 (1952)

16. R. O. Haxer and L. Katz, Canadian, 11, No.9
14 (1958)

Thesis 28783
S221 Sawtelle
Measurement of the
Bremsstrahlung spectrum of
the linear accelerator.

Thesis 28783
S221 Sawtelle
Measurement of the Bremsstrahlung
spectrum of the linear accelerator.

thesS221
Measurement of the bremsstrahlung spectr
3 2768 002 00290 9
DUDLEY KNOX LIBRARY